Supplement of Proc. IAHS, 382, 285–290, 2020
https://doi.org/10.5194/piahs-382-285-2020-supplement

Supplement of

Factors controlling natural subsidence in the Po Plain

Luigi Bruno et al.

Correspondence to: Luigi Bruno (luigibruno@unimore.it)

Supplementary data

Radiocarbon dates

Chronological constrain for core correlation is provided by 28 published ^{14}C ages (Sheets 204 and 222 of the Geological Map of Italy to scale 1:50000; Amorosi et al., 2005; Amorosi et al., 2017; Bruno et al., 2017) and from 48 ^{14}C dates carried out at the at the KIGAM Laboratory (Korea Institute of Geoscience and Mineral Resources, Daejeon, Republic of Korea). Conventional ^{14}C ages (S1) were calibrated using OxCal 4.2 (Bronk Ramsey & Lee, 2013) with the IntCal 13 and Marine13 curves (Reimer et al., 2013).

Core	Sample depth (m)	Sample code	C14 age	Cal year BP (mean value)	Material	References	Figure
B2	5.8	KGM-TWd180568b	320±20	380±40	Peat	This paper	4
	11.15	KGM-TWd180570a	650±30	610±40	Wood	This paper	3,4
	12.35	KGM-TWd180571a	730±20	680±10	Wood	This paper	4
	13.8	KGM-TWd180572a	960±40	860±50	Wood	This paper	3,4
	15-3	KGM-TWd180574a	1190±20	1120±40	Peat	This paper	3,4
	16.6	KGM-TWd180575a	2730±30	2820±30	Wood	This paper	3
	17.6	KGM-TWd180576a	3820±30	4220±60	Peat	This paper	3
	19.2	KGM-TCa180070a	5030±30	5530±40	Shell	This paper	3,4
	20.25	KGM-TWd180577a	5390±30	6210±60	Wood	This paper	3,4
	21.6	KGM-TWd180578a	7150±30	7970±20	Peat	This paper	3,4
	22.05	KGM-TSa180035a	9500±40	10840±130	Bulk sediment	This paper	3,4
	29.8	KGM-TSa180036a	246300±90	28660±120	Bulk sediment	This paper	3,4
B3	3.55	KGM-TWd190145	2120±20	2090±40	Peat	This paper	3,4
	3.95	KGM- TWd190146	3020±30	3210±60	Peat	This paper	4
	4.35	KGM- TWd190147	4250±40	4830±70	Wood	This paper	4
	5.95	KGM- TWd190148	4500±30	5170±80	Wood	This paper	3,4
	6.6	KGM- TWd190149	4910±30	5630±30	Wood	This paper	3,4
	6.95	KGM- TWd190150	5330±30	6110±60	Peat	This paper	3,4
	7.9	KGM- TWd190151	6280±30	7210±30	Plant fragment	This paper	3,4
	8.5	KGM- TWd190152	6480±30	7380±40	Peat	This paper	4
	8.67	KGM- TWd190153	6780±30	7630±20	Peat	This paper	4
	9.08	KGM- TWd190154	7130±40	7960±40	Peaty clay	This paper	4
	9.2	KGM-TSa190025	8870±50	10000±120	Bulk sediment	This paper	3,4
	12.6	KGM- TSa190026	23750±140	27820±130	Bulk sediment	This paper	3,4
	15.6	KGM- TSa190028	28590±200	32630±370	Organic Clay	This paper	3,4
B4	5.15	KGM- TWd190155	1780±20	1700±50	Peat	This paper	3,4
	6.05	KGM- TWd190156	2770±30	2860±40	Peat	This paper	3,4

	6.36	KGM- TWd190157	3230±30	3450±40	Wood	This paper	4
	6.9	KGM- TWd190158	4070±30	4560±90	Wood	This paper	4
	8.4	KGM- TWd190159	4180±30	4720±60	Wood	This paper	3,4
	9.58	KGM- TWd190161	5240±30	5980±70	Peat	This paper	4
	10.1	KGM- TWd190162	5290±30	6080±60	Peat	This paper	3,4
	10.9	KGM- TWd190163	6120±30	7000±70	Peat	This paper	4
	11.85	KGM- TWd190164	6440±30	7370±40	Wood	This paper	4
	12.4	KGM- TWd190165	6470±30	7380±30	Wood	This paper	3,4
	15.5	KGM- TWd190166	8710±40	9650±80	Wood	This paper	Supp. Mat.
	15.6	KGM- TSa190029	9780±60	11200±70	Organic Clay	This paper	3,4
	21.3	KGM- TWd190167	22710±90	27080±170	Peat	This paper	3,4
	24.96	KGM- TSa190030a	28660±210	32740±380	Organic Clay	This paper	3,4
	30.85	KGM- TSa190031	40130±450	43760±420	Organic Clay	This paper	3,4
EM 1	5.75	KGM-OWd150177	2680±40	2970±110	Peat	Amorosi et al., 2017	3,4
	9.50	KGM-OWd150178	4190±40	4690±85	Plant fragment	Amorosi et al., 2017	3,4
	11.30	KGM-OWd150179	5630±40	6150±130	Shell	Amorosi et al., 2017	4
	11.40	KGM-OWd150180	5340±40	6105±110	Wood	Amorosi et al., 2017	3,4
	13.30	KGM-OWd150181	6340±50	7250±85	Plant fragment	Amorosi et al., 2017	3,4
	16.50	KGM-OWd160062	7040±50	7870±50	Peat	Amorosi et al., 2017	3,4
	17.85	KGM-OWd150182	7340±50	8125±105	Wood	Amorosi et al., 2017	4
	18.40	KGM-OWd160063	7730±50	8510±50	Peat	Amorosi et al., 2017	3,4
	18.70	KGM-OSn150001	9950±60	11430±195	Organic clay	Amorosi et al., 2017	3,4
	25.3	KGM-TSa180006	22190±100	26400±160	Wood	This paper	3,4
	26.90	KGM-OWd150183	22200±120	26450±390	Wood	Amorosi et al., 2017	4
	30.1	KGM-TSa180007	27810±150	31520±190	Peaty clay	This paper	3,4
EM 8	5.45	OWd160064	4890±50	5630±50	Wood	Bruno et al., 2017	3
	7.3	OWd160065	5800±40	6600±50	Wood	Bruno et al., 2017	3
	22.4	OWd160066	7950±40	8820±100	Wood	Bruno et al., 2017	3
187 S1	7.95	KGM-TCa180071	1860±30	1270±40	Shell	Amorosi et al., 2019	3
	15.90	KGM-TCa180072	2340±30	1800±50	Shell	Amorosi et al., 2019	3
	19.75	KGM-TWd180579	2570±20	2070±60	Wood	Amorosi et al., 2019	3
	25.85	Beta Analytic-187 S1_25.85	8250±60	9230±100	Plant fragment	CARG Project, Sheet 187	3
	50.05	Beta Analytic-187 S1_50.05	41750±1000	45700±1900	Peat	CARG Project, Sheet 187	3

204 S4	21	ENEA-204 S4_26.8	35500±3000	41730±6620	Organic clay	CARG Project, Sheet 204	3
204 S5	8.50	KGM-OWd170593-1	3910±30	4345±50	Plant fragment	Bruno et al., 2019	4
	9.30	KGM-OWd170594-1	4390±30	4955±60	Plant fragment	Bruno et al., 2019	3
	10.30	KGM-OWd170595-1	5140±30	5620±30	Plant fragment	Bruno et al., 2019	3
	16.95	ETH-204S5_16.95	7735±70	8520±70	Wood	Amorosi et al., 2005	3
	22.70	ETH-204S5_22.7	23320±210	27545±155	Peat	CARG Project, Sheet 204	4
204 S17	12,8	KGM-OWd170597-1	3850±30	4270±70	Plant fragment	This paper	3,4
	13.40	KGM-OWd170598-1	3930±30	4370±60	Plant fragment	This paper	4
	14.75	KGM-OWd170599-1	5170±30	5630±30	Plant fragment	This paper	3,4
	14.95	KGM-OWd170600-1	5530±30	6100±60	Plant fragment	This paper	4
	17	KGM-OWd170601-1	6840±30	7670±30	Plant fragment	This paper	3,4
222 S2	7.0	Beta Analytic-222 S2_7.0	340±60	400±40	Peat	CARG Project, Sheet 222	3
	17.0	Beta Analytic-222 S2_17.0	6000±60	6850±40	Peat	CARG Project, Sheet 222	3
	20.9	Beta Analytic-222 S2_20.9	7420±60	8270±40	Organic Clay	CARG Project, Sheet 222	3
	26.2	Beta Analytic-222 S2_26.2	19770±150	23660±490	Peat	CARG Project, Sheet 222	3

S1. List of radiocarbon dates

Decompaction model

Decompacted thickness H_0 of a soil column presently comprised between depth z_1 and z_2 can be computed as (Gambolati et al., 1998):

$$H_0 = (1 + e_0) \int_{z_1}^{z_2} \frac{dz}{1 + e(z)}$$

where e_0 initial void index and $e(z)$ is the void index at depth z. The behavior of $e(z)$ in virgin loading conditions is given by

$$e(z) = e_0 - C_c \log \sigma_z$$

with C_c the compression index and σ_z the intergranular effective stress.

Application of decompaction model to core B4

The above described decompaction model was applied to core B4 (S2) where six depositional facies association were identified. The reader is referred to Amorosi et al. (2005 2017a, b), Bruno et al. (2017) and Giacomelli et al. (2018) for detailed description. A brief description is provided in S3, together with geothecnical parameters e_0 and C_c.

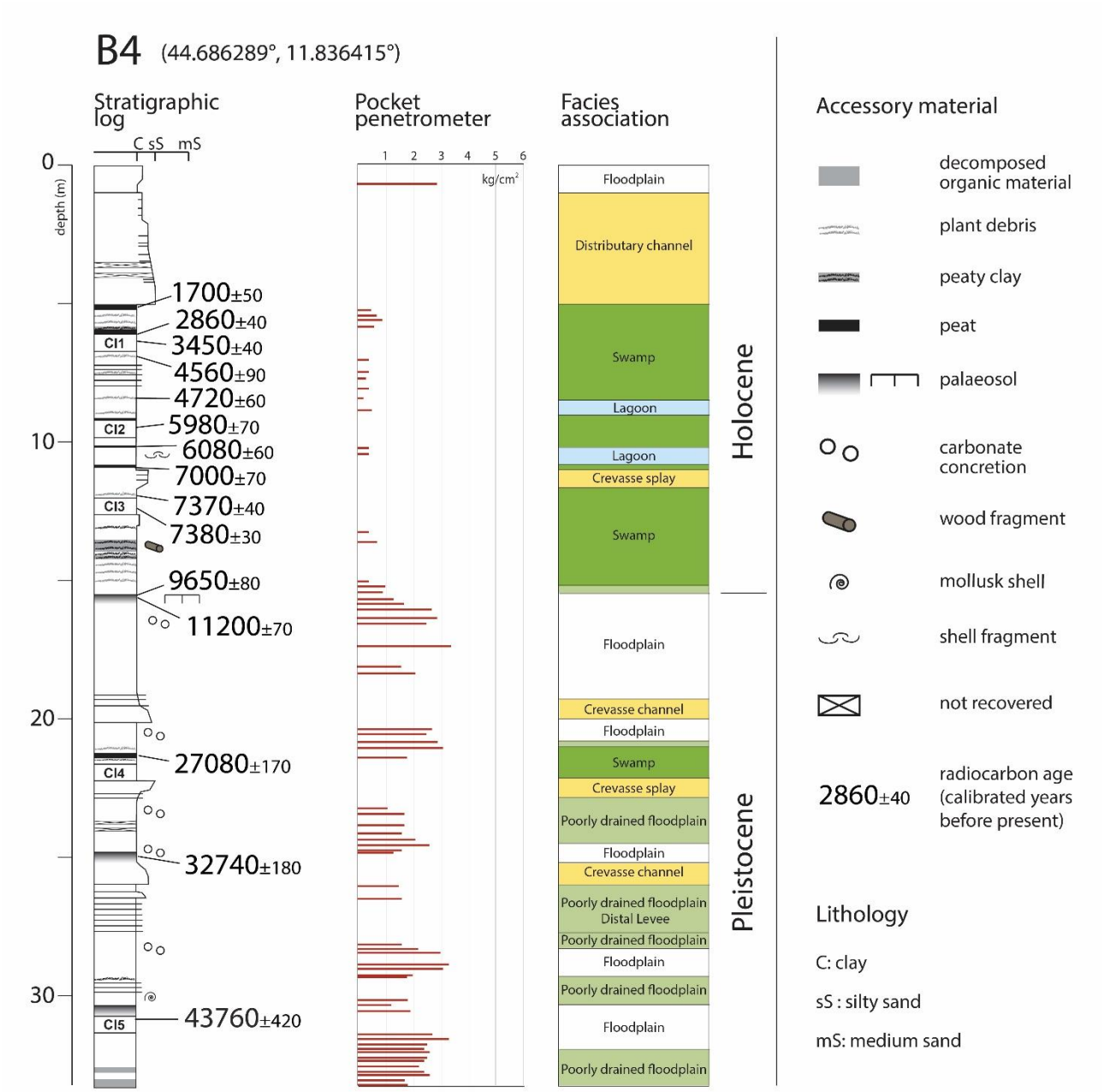

S2. Stratigraphic log of core B4

Geothecnical characterization of facies associations was based on; (i) loss on ignition and bulk density determination carried out on 6 undisturbed samples from core B4 (ii) 22 oedometer tests carried out on nearby cores from the database of the Geological Seismic and Soil Survey of Regione Emilia Romagna.

Depositional system	facies association	lithology	Accessory material, sedimentary structures	PP	e0	cc
Lowed delta plain – outer estuary	Lagoon	silty clay	Brackish fossils	< 1.2	1.56	0.15
Upper delta plain – inner estuary	Swamp	peat	Wood, plant debris	-	2.29	0.86
		clay	Freshwater to low brackish fossils, plant debris	< 1.2	1.56	0.15
	Poorly drained floodplain	silty clay	Parallel lamination	1.2 – 1.8	0.99	0.23
Alluvial Plain	Floodplain	clayey silt	carbonate concretions, Fe and Mn oxides	> 1.8	0.84	0.12
	Crevasse and levee	silty sand	Parallel and cross lamination	-	0.42	0.17

S3. Geomechanical parameters e_0 and C_c used to decompact the units of core B4. PP = pocket penetrometer.

A simplified stratigraphy was used for decompaction of core B4 (S4). The deformation of each unit is computed as $(H_0 - H)/H_0$, with H the actual thickness of the unit. The higher compaction is associated with the peat horizons.

Facies association	H (m)	H0 (m)	Deformation (%)
Crevasse and levee	4.15	5.14	19.26
Swamp peat	0.10	0.19	47.09
Swamp clay and lagoon	4.23	4.76	11.13
Swamp peat	0.10	0.21	51.92
Lagoon	1.32	1.50	12.00
Crevasse and levee	0.95	1.26	24.60
Swamp clay	2.25	2.57	12.45
Poorly drained floodplain	1.40	1.87	25.13
Floodplain	5.30	6.22	14.79
Swamp peat	0.55	1.56	64.74
Poorly drained floodplain	3.50	4.93	29.01
Floodplain	6.00	7.16	16.20

S4. Result of the decompaction model for each unit of core B4. Boulder line marks the Pleistocene/Holocene boundary

References

Amorosi, A., Centineo, M.C., Colalongo, M.L. and Fiorini, F.: Millennial-scale depositional cycles from the Holocene of the Po Plain, Italy, Marine Geology, 222-223, 7-18, doi:10.1016/j.margeo.2005.06.041, 2005.

Amorosi, A., Bruno, L., Campo, B., Morelli, A., Rossi, V., Scarponi, D., Bohacs, K.M and Drexler, T. M.**:** Global sea-level control on local parasequence architecture from the Holocene record of the Po Plain, Italy, Marine and Petroleum Geology, 87, 99–111, doi.org/10.1016/j.marpetgeo.2017.03.03, 2017a

Amorosi, A., Bruno, L., Cleveland, D.M., Morelli, A. and Hong, W.**:** Paleosols and associated channel-belt sand bodies from a continuously subsiding late Quaternary system (Po Basin, Italy): New insights into continental sequence stratigraphy. Geological Society of America Bulletin, 129(3), 1-15, doi: 10.1130/B31575.1, 2017b.

Amorosi A., Bruno L., Campo B., Costagli B., Dinelli E., Hong W., Sammartino I. and Vaiani S.C.: Tracing clinothem geometry and sediment pathways in the prograding Holocene Po Delta system through integrated core stratigraphy, Basin Research, doi.org/10.1111/bre.12360, 2019.

Bronk Ramsey, C. and Lee, S.: Recent and planned developments of the program OxCal, Radiocarbon, 55(2–3), 720–730, doi:10.2458/azu_js_rc.55.16215, 2013.

Bruno, L., Bohacs, K. M., Campo, B., Drexler, T. M., Rossi, V., Sammartino, I. and Amorosi, A.: Early Holocene transgressive paleogeography in the Po coastal plain (Northern Italy), Sedimentology, 64(7), 1792–1816, doi:10.1111/sed.12374, 2017.

Gambolati, G., Giunta, G. and Teatini, P.: Numerical modeling of natural land subsidence over sedimentary basins undergoing large compaction. In: Gambolati, G. (Ed.), CENAS - Coastiline Evolution of the Upper Adriatic Sea due to Sea Level Rise and Natural and Anthropogenic Land Subsidence. Klwer Acedemic Publ., 28 (4), 77–102, 1998.

Giacomelli S., Rossi, V., Amorosi, A., Bruno, L., Campo, B., Ciampalini, A., Civa, A., Hong, W., Sgavetti, M. and de Souza Fiho, C.R.: A mid-late Holocene tidlly-influenced drainage system revealed by integrated remote sensing, sedimentological and stratigraphic data, Geomorphology 318, 421-436, doi:10.1016/j.geomorph.2018.07.004, 2018.

Reimer, P. J., Bard, E., Bayliss, A., Beck, J. W., Blackwell, P. G., Ramsey, C. B. and van der Plicht, J.: IntCal13 and Marine13 radiocarbon age calibration curves, 0–50,000 years cal BP, Radiocarbon, 55, 1869–1887, doi.org/10.2458/azu_js_rc.55.16947, 2013.